Received: 10 October 2016 | Accepted: 14 October 2016

DOI 10.1111/cmi.12685

WILEY

RESEARCH ARTICLE

Analysis of Ca^{2+} mediated signaling regulating *Toxoplasma* infectivity reveals complex relationships between key molecules

Rebecca J. Stewart[1,2] | Lachlan Whitehead[1,2] | Brunda Nijagal[3] | Brad E. Sleebs[1,2] | Guillaume Lessene[1,2,4] | Malcolm J. McConville[5] | Kelly L. Rogers[1,2] | Christopher J. Tonkin[1,2]

[1] The Walter and Eliza Hall Institute of Medical Research, Parkville, Victoria, Australia

[2] Department of Medical Biology, The University of Melbourne, Melbourne, Victoria, Australia

[3] Metabolomics Australia, Bio21 Molecular Science and Biotechnology Institute, University of Melbourne, Parkville, Victoria, Australia

[4] Department of Pharmacology and Therapeutics, The University of Melbourne, Melbourne, Victoria, Australia

[5] Department of Biochemistry and Molecular Biology, Bio21 Molecular Science and Biotechnology Institute, The University of Melbourne, Parkville, Australia

Correspondence
Chris Tonkin, Division of Infection and Immunity, The Walter and Eliza Hall Institute of Medical Research, 1G Royal Parade, Parkville 3052, Victoria, Australia.
Email: tonkin@wehi.edu.au

Funding information
Australian Cancer Research Foundation, National Health and Medical Research Council (NHMRC), Grant/Award Number: GNT1017059. GNT1047806. GNT1022559. Australian Research Council (ARC) Future Fellowship, Grant/Award Number: FT120100164.

Abstract

Host cell invasion, exit and parasite dissemination is critical to the pathogenesis of apicomplexan parasites such as *Toxoplasma gondii* and *Plasmodium* spp. These processes are regulated by intracellular Ca^{2+} signaling although the temporal dynamics of Ca^{2+} fluxes and down-stream second messenger pathways are poorly understood. Here, we use a genetically encoded biosensor, GFP-Calmodulin-M13–6 (GCaMP6), to capture Ca^{2+} flux in live *Toxoplasma* and investigate the role of Ca^{2+} signaling in egress and motility. Our analysis determines how environmental cues and signal activation influence intracellular Ca^{2+} flux, allowing placement of effector molecules within this pathway. Importantly, we have identified key interrelationships between cGMP and Ca^{2+} signaling that are required for activation of egress and motility. Furthermore, we extend this analysis to show that the Ca^{2+} Dependent Protein Kinases–*Tg*CDPK1 and *Tg*CDPK3—play a role in signal quenching before egress. This work highlights the interrelationships of second messenger pathways of *Toxoplasma* in space and time, which is likely required for pathogenesis of all apicomplexan species.

1 | INTRODUCTION

Malaria and toxoplasmosis are caused by infection with the apicomplexan parasites *Plasmodium* and *Toxoplasma*, respectively. Malaria kills more than 700,000 people annually, while *Toxoplasma* chronically infects 30% of world's population and can cause birth defects, blindness, and disease in immunocompromised individuals (World Health Organization, 2014; Pappas et al., 2009). These ancient parasites have evolved mechanisms to sense their environment responding to cues to activate host cell invasion, intracellular replication, egress, and motility for parasite dissemination, a process collectively termed the lytic cycle. External cues activate parasite signaling cascades, most notably Ca^{2+} signaling, to drive progress through the lytic cycle including transitions from intracellular replication to extracellular motility (For review see (Lourido & Moreno, 2015)). Specifically, Ca^{2+} signaling controls the regulated release of specialized organelles called micronemes, which harbor adhesins and other factors required for invasion and egress that are central to apicomplexan pathogenicity (Carruthers & Sibley, 1999; Lovett, Marchesini, Moreno, & Sibley, 2002; Wetzel, Chen, Ruiz, Moreno, & Sibley, 2004). Parasite motility is also thought to be regulated by Ca^{2+} signaling via activation of the 'glideosome'—an actomyosin motor which provides the force

required for a distinctive form of cellular locomotion termed 'gliding motility'. However, little is understood about the spatio-temporal dynamics and hierarchy of signaling pathways and how key molecules relate to one another during motility and egress.

The cyclic nucleotide second messenger, cyclic GMP (cGMP), activates Protein Kinase G (PKG), and also plays a vital role in the activation of apicomplexan egress, motility and differentiation (Wiersma et al., 2004; Eaton, Weiss, & Kim, 2006; Taylor, McRobert, & Baker, 2008; Collins et al., 2013). cGMP signaling is tightly regulated by guanylyl cyclases and phosphodiesterases (PDEs) that are responsible for *de novo* synthesis and degradation of cGMP, respectively. As a result, targeted inhibition of parasite PDEs with zaprinast or 5-benzyl-3-isopropyl-1H-pyrazolo[4.3-*d*]pyrimindin-7(6H)-one (BIPPO) prevents cGMP breakdown leading to an accumulation of cellular cGMP, which activates PKG and in turn signals for microneme secretion and egress (Howard et al., 2015). Conversely, inhibition of PKG interrupts cGMP signaling leading to microneme secretion defects in both *Toxoplasma* and *Plasmodium* spp. (Wiersma et al., 2004; Donald et al., 2006; Collins et al., 2013). Recent work suggests that this pathway plays a role in regulating of phosphoinositide metabolism and Ca^{2+} signaling during stage conversion and motility in *Plasmodium* (Brochet et al., 2014) and Ca^{2+} signaling driving microneme secretion during the asexual cycle of *Toxoplasma* (Brown, Lourido, & Sibley, 2016, Sidik et al., 2016).

Apicomplexa have evolved divergent signaling elements to regulate novel functions specific to this group of pathogens. Plant-like Ca^{2+} dependent proteins kinases (CDPKs) are expanded across Apicomplexa and play pivotal roles in Ca^{2+} signal transduction throughout the lytic cycle (For review see (Billker, Lourido, & Sibley, 2009)). CDPKs contain Ca^{2+} binding EF hand domains fused with a calmodulin-like kinase domain and inhibitory region, an architecture seen only in protists and plants and not metazoans. Upon interactions with Ca^{2+} ions, conformational change relieves autoinhibition and reveal the active site for substrate phosphorylation (Wernimont et al., 2010). CDPKs have been implicated in a range of processes, including stage conversion (Billker et al., 2004; Sebastian et al., 2012; Brochet et al., 2014), invasion (Lourido et al., 2010; Bansal et al., 2013) and egress (Dvorin et al., 2010; McCoy, Whitehead, van Dooren, & Tonkin, 2012; Garrison et al., 2012; Lourido, Tang, & Sibley, 2012). In the case of *Tg*CDPK1, this kinase plays a role in regulation of adhesins from the microneme organelles (Lourido et al., 2010). Despite the multifaceted role of Ca^{2+} signaling in Apicomplexan parasites little is known about how Ca^{2+} signaling operates, in space and time, to activate these kinases.

In mammalian cells, Ca^{2+} signal transduction commonly involves the regulated release of Ca^{2+} from intracellular stores (i.e., ER) into the cytoplasm (Berridge, 2009). Regulated pump and channel activation drive distinct spatiotemporal Ca^{2+} oscillatory patterns modulating amplitude, duration, and localization for diverse cellular outcomes (Berridge, Bootman, & Roderick, 2003; Uhlen & Fritz, 2010). This phenomenon has been documented in *Toxoplasma* where cytoplasmic Ca^{2+} flux coincides with a burst of parasite motility immediately preceding invasion (Lovett, 2003). However, studies such as these have been technically limited due the broad cellular targeting of Ca^{2+} sensitive dyes. The development of genetically encoded Ca^{2+} sensors has revolutionized the understanding of signaling processes in living cells (Chen et al., 2013). In the case of Apicomplexa, the focused expression of the genetically encoded Ca^{2+} sensors has allowed for the differentiation between signals derived from the host and those initiated by the occupying parasites (Borges-Pereira et al., 2015). Interestingly, the source of intracellular Ca^{2+} has been brought into question through use of GCaMPs identifying a PKG regulated neutral Ca^{2+} store distinct from the ER (Sidik et al., 2016).

In this study, we examine the spatiotemporal dynamics of intracellular signal transduction and investigate the interplay of multiple signaling nodes in *Toxoplasma* egress and motility. We employ the genetically encoded Ca^{2+} indicator GCaMP6s (Chen et al., 2013), and the new cGMP agonist, BIPPO (Howard et al., 2015), to interrogate the hierarchy of signal transduction pathways, identifying activation of cGMP upstream of Ca^{2+} in both egress and motility. Extending this approach to CDPKs, we reveal a role for *Tg*CDPK1 and *Tg*CDPK3 in Ca^{2+} levels immediately prior to egress. Furthermore, we demonstrate the relationship of Ca^{2+} periodicity and amplitude as a driver of speed and distance travelled by motile parasites, thus together revealing the importance of Ca^{2+} signaling as a key mediator of *Toxoplasma* infectivity.

2 | RESULTS

2.1 | GCaMP6s detects parasite-derived Ca^{2+} during *Toxoplasma* motility and egress

We sought to monitor intracellular Ca^{2+} flux within live tachyzoites using the genetically encoded, Ca^{2+} biosensor GCaMP6s (Chen et al., 2013). For ratiometric analysis in *Toxoplasma*, we co-expressed mCherry with GCaMP6s, whilst integration into the *uprt* locus ensured consistent expression across cell lines (Figure 1a). Visualization of these lines demonstrated that both fluorescent signals could be detected in the cytoplasm of live extracellular and intracellular tachyzoites (Figure 1b).

Ca^{2+} signaling can result from release of Ca^{2+} from internal stores, and/or influx from extracellular sources (Berridge, 2009; Uhlen & Fritz, 2010). To assess the contribution of internal Ca^{2+} stores for signaling in *Toxoplasma* motility GCaMP6s-expressing tachyzoites were harvested in modified Ringer's + EGTA (0.1 mM) solution away from host cells. Under resting conditions, nonmotile parasites exhibited low cytoplasmic Ca^{2+} levels (Figure 1c, no stimulation—60s time lapse projection, Ca^{2+} false colored low = blue and high = red). In the absence of extracellular Ca^{2+}, the Ca^{2+} ionophore A23187 robustly activated Ca^{2+} signaling and motility of tachyzoites (Figure 1c, A23187–lower panel) (Movie S1). Further, ratiometric quantitation showed rapid induction of cytoplasmic Ca^{2+} with the population average increasing poststimulation (Figure 1d). Autofluorescence of A23187 was found not to influence our readings (Supplementary Figure 1a). Tachyzoite motility was strongly correlated with GCaMP6s fluorescence with ~60% of ionophore treated parasites exhibiting movement in the 60s following Ca^{2+} increase (Figure 1e; motility discussed further in Figures 6 and 7) (Movie S1). This analysis demonstrates the capacity of GCaMP6s to measure tachyzoites ability to store and respond to endogenous Ca^{2+} signaling in the absence of external Ca^{2+} sources.

Unlike Ca^{2+} sensitive dyes, the use of genetically encoded Ca^{2+} biosensors, such as GCaMP6s, allows detailed assessment of individual

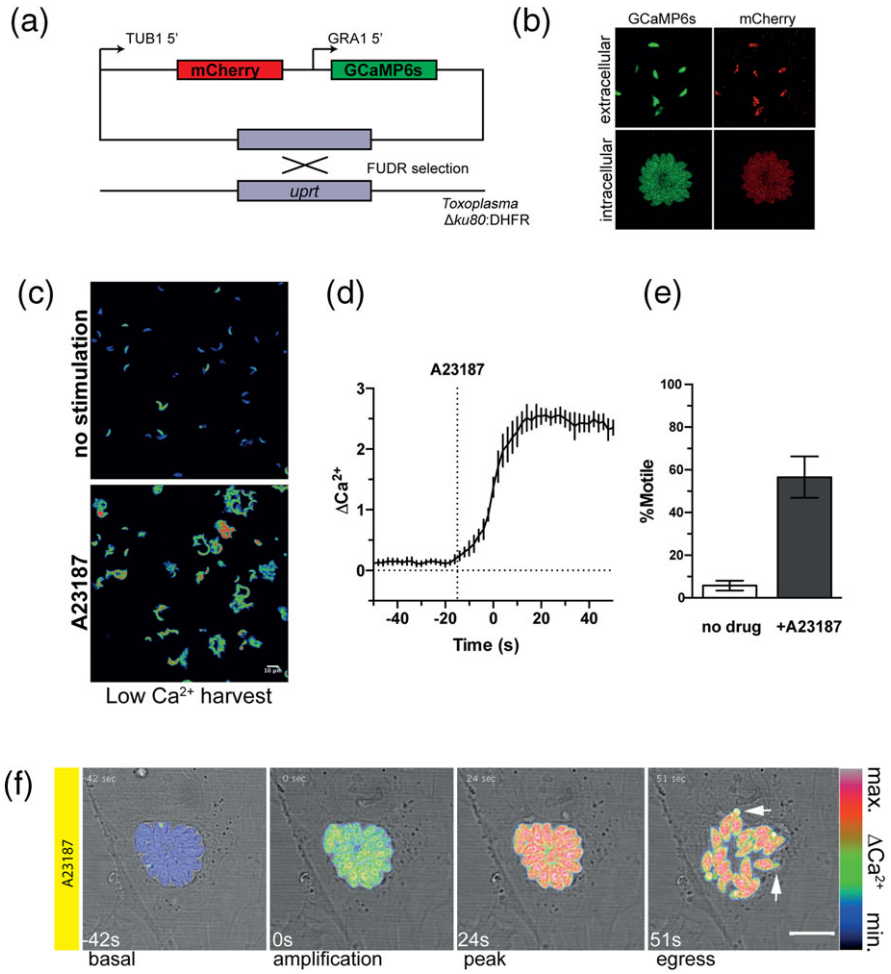

FIGURE 1 GCaMP6s can detect changes in intracellular Ca^{2+} of *Toxoplasma*. (a) Genetic strategy for expression GCaMP6s/mCherry integrated as a single copy into *uprt* of tachyzoites. (b) GCaMP6s and mCherry are expressed and localized to the tachyzoite cytoplasm in extracellular and intracellular tachyzoites. GCaMP6s = green, mCherry = red. (c) Validation of GCaMP6s for monitoring release of intracellular Ca^{2+} stores. Tachyzoites were harvested in modified Ringer's buffer (+0.1 mM EGTA) to remove external Ca^{2+} sources and then stimulated with A23187. Ca^{2+} response false colored where blue = low Ca^{2+} and red = high Ca^{2+}. Scale bar = 10 μm here and throughout. (d) Tracking of Ca^{2+} response before and after A23187 addition shows a twofold to threefold change in Ca^{2+} signaling as determined by ratiometric analysis of ΔCa^{2+} (GCaMP6s/mCherry, normalized to 0). (e) Motility change accompanying Ca^{2+} responses in absence of environmental Ca^{2+} shows an average of 60% of tachyzoites engaging motility after A23187 stimulation −/+s.e.m, $n = 4$. (f) Basal intracellular tachyzoites maintain low Ca^{2+} levels. A23187 treatment stimulates amplification of the Ca^{2+} signal, peaking prior to parasite egress as detected with our GCaMP6s approach

intracellular tachyzoites. We therefore monitored Ca^{2+} dynamics of intracellular tachyzoites at the single vacuole level within host cells in unstimulated and activated states. Basal, intracellular parasites maintained low Ca^{2+} levels (Figure 1f, basal panel). Upon stimulation with A23187, cytoplasmic Ca^{2+} rapidly increased followed by parasite egress from host cells (Figure 1f, amplification, peak, and egress) (Movie S2). This assessment of live Ca^{2+} flux defines two states; (a) an immotile, low Ca^{2+} state of intracellular tachyzoites and (b) an active, motile state where rapid induction of Ca^{2+} drives parasite egress for extracellular dissemination. Together, this work validates GCaMP6s for Ca^{2+} detection and analysis in *Toxoplasma* egress and motility.

2.2 | cGMP signaling through PKG precedes Ca^{2+} signaling in egress

Recent work has suggested the importance of cGMP pathway and its link with Ca^{2+} signaling (Brochet et al., 2014; Brown et al., 2016; Sidik et al., 2016); however, this work relied on the use of a human PDE inhibitor zaprinast. Here, activation of egress by zaprinast requires long incubation times and high concentrations, often resulting in heterogeneous responses (Howard et al., 2015). We recently described a potent, apicomplexan-specific PDE inhibitor, BIPPO. BIPPO shows high selectivity to towards *Toxoplasma* and *P. falciparum* PDE and rapidly induces host cell egress and microneme secretion in a PKG dependent manner (Howard et al., 2015). To determine first whether treatment with BIPPO induces an increase in cyclic nucleotide production, we measured cAMP and cGMP levels using LC–MS (Figure 2a). Extracellular tachyzoites were treated with either 1 μM of BIPPO or 2 μM of the Ca^{2+} ionophore A23187 for 1 min followed by rapid quenching. Levels of the cyclic nucleotides, cGMP and cAMP, were expressed relative to their nucleotide triphosphate counterparts, GTP and ATP, respectively. This analysis showed that BIPPO treatment elicited a rise in levels of both cGMP and cAMP as compared to DME growth media alone. The Ca^{2+} ionophore A23187 also caused a rise in these cyclic nucleotides (Figure 2ai, ii).

We then used BIPPO to explore the relationship of cGMP and Ca^{2+} signaling. We monitored Ca^{2+} dynamics of tachyzoites induced to egress with BIPPO and showed a clear amplification of cytoplasmic Ca^{2+} concentrations prior to parasite egress (Figure 2bi) (Movie S3). By performing ratiometric analysis and normalizing the GCaMP6s signal to mCherry fluorescence, we analysed specific aspects of the Ca^{2+} response and compared these dynamics across multiple conditions. In the case of BIPPO stimulation of WT cells, all tachyzoites responded with robust amplification of Ca^{2+} before egressing within 75 s of the first instance of Ca^{2+} increase (Figure 2bii–response normalized to ½ peak Ca^{2+} as $t = 0$ s, one line represents one vacuole and ceases at the point of egress). This demonstrates that activation of cGMP is linked to Ca^{2+} signaling in activating egress. Given that BIPPO induces a rise in both cGMP and cAMP, we further explored the link between cGMP and Ca^{2+} by inhibiting PKG. PKG is a cGMP-dependent protein

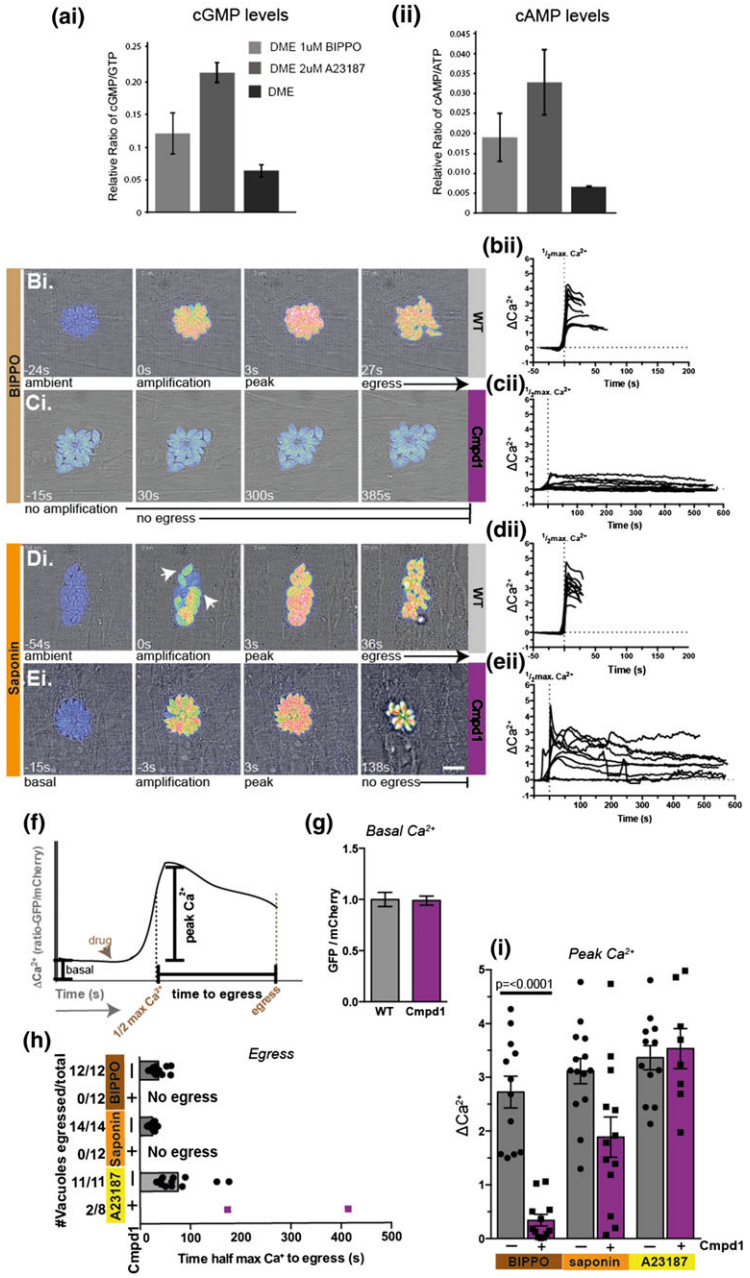

FIGURE 2 Protein Kinase G is required for Ca^{2+} signaling and egress in *Toxoplasma*. (a). Relative levels of (i) cGMP and (ii) cAMP upon 1 μM BIPPO and 2 μM of A23187. *n* = 2–3, −/+s.e.m (bi) Induction of cGMP signaling using BIPPO activates cytoplasmic Ca^{2+} signaling within *Toxoplasma* prior to egress. (bii) Ratiometric analysis of Ca^{2+} responses to BIPPO confirms rapid amplification of Ca^{2+} levels before peaking prior to egress. Here and throughout ratiometric analysis is displayed as: one line = one vacuole, analysis ceases at point of egress, ×-axis = ΔCa^{2+} as GCaMP6s/mCherry normalized to half max Ca^{2+}, *y*-axis = normalized to GCaMP6s/mCherry = t_0. *n* = 12 vacuoles. (ci) PKG inhibition by Cmpd1 blocks cGMP signal transduction preventing BIPPO induced Ca^{2+} response and egress of intracellular tachyzoites. (cii) Ratiometric analysis confirms inability of Cmpd1 treated cells to engage Ca^{2+} signaling in response to BIPPO. *n* = 12, filmed up to 10 min. (di) Host cell permeabilisation with saponin leads to a rise in intracellular Ca^{2+} and activation of egress. Ca^{2+} activation is not uniform across tachyzoites within individual vacuoles displaying differential Ca^{2+} amplification before reaching peak Ca^{2+} followed by egress (amplification, arrows). (dii) Ratiometric analysis shows rapid amplification of Ca^{2+} signaling in response to saponin treatment, reaching a peak before a short period of Ca^{2+} dampening preceding egress. (ei) Inhibition of PKG by Cmpd1 prevents saponin-induced egress but tachyzoites still show variable Ca^{2+} responses indicating alternate Ca^{2+} activation mechanisms independent of PKG signaling. (eii) Ratiometric analysis demonstrates initial peak of Ca^{2+} levels followed by dynamic Ca^{2+} response to saponin in Cmpd1 treated cells, but egress does not occur. (f) Schematic of Ca^{2+} metrics investigated by ratiometric analysis; basal Ca^{2+}, time to egress and peak Ca^{2+} ratio. (g) Basal Ca^{2+} levels of resting intracellular vacuoles assessed as GCaMP6s/mCherry ratio, measured over 15 s, normalized to 1 = WT average. No difference was detected between basal Ca^{2+} of WT and Cmpd1 treated tachyzoites. *n* = 12, −/+ s.e.m. (h) WT parasites egressed within 100 s of BIPPO, saponin or A23187 stimulation. Cmpd1 treated tachyzoites show defective activation with no egress seen for BIPPO and saponin stimulation. (i) Analysis of Peak Ca^{2+} ratio derived from ratiometric analysis compared across −/+Cmpd1 stimulated with BIPPO, saponin and A23187. Quantitation demonstrates a defect in Ca^{2+} induction with BIPPO stimulation of Cmpd1 treated cells. Although Peak Ca^{2+} is retained in Cmpd1 treated cells activated with saponin and A23187 this Ca^{2+} signaling is not sufficient for egress without cGMP signaling through PKG. *n* = 8–14 vacuoles, −/+ s.e.m

kinase and in apicomplexan parasites can be specifically inhibited by the trisubstituted pyrrole termed 'Compound 1' (Cmpd1; Donald & Liberator, 2002). Upon treatment of GCaMP6s expressing tachyzoites with Cmpd1 parasites failed to mount a Ca^{2+} response and could not activate motility or egress, remaining intracellular for the duration of filming, up to 10 min (Figure 2ci, ii) (Movie S4). Indeed, this work is consistent with other studies showing that zaprinast can induce Cmpd-1 dependent increase in Ca^{2+} (Sidik et al., 2016). Together, this work supports the role of cGMP in activating Ca^{2+} signaling through the action of PKG during egress of *Toxoplasma*.

Toxoplasma tachyzoites also egress in response to changes in extracellular [K^+] and pH, which may signal immune attack or a dying host cell (Black, Arrizabalaga, & Boothroyd, 2000; Persson et al., 2007; Roiko, Svezhova, & Carruthers, 2014). To investigate the impact of these signals on parasite Ca^{2+} fluxes, the membrane of host cells was selectively permeabilized with saponin (Carruthers & Sibley, 1997). When intracellular parasites were treated with saponin, whilst in a low [K^+] buffer, tachyzoites displayed a rise in cytoplasmic Ca^{2+}, however, as compared to A23187 and BIPPO treated tachyzoites, the increase in cytoplasmic Ca^{2+} was not uniform across the vacuole. Rather parasites individually activated Ca^{2+} responses over 3–5 s (Figure 2di arrows) until all intracellular parasites within the same vacuole displayed high Ca^{2+} prior to egress (Figure 2di, ii) (Movie S5). To make sure the saponin was not activating tachyzoite motility by directly acting on the parasite in an unknown fashion extracellular tachyzoites were treated with this detergent and GCaMP6s fluorescence measured. Here, saponin was unable to induce a rise in GCaMP6s fluorescence not induce parasite motility in the presence of Ca^{2+} (Supplementary Figure 1d and e). To define the relationship between extracellular cues, intracellular cGMP, and Ca^{2+} during egress under these conditions, we inhibited *Toxoplasma* PKG with Cmpd1 before activating egress with saponin, while monitoring the Ca^{2+} responses. Here, in direct contrast to activation with BIPPO, saponin treatment induced a rise in Ca^{2+} although parasites did not activate motility or egress, remaining intracellular for the duration of filming (Figure 2ei, ii) (Movie S6).

To understand in more detail, the effect of stimuli on Ca^{2+} signaling, we interrogated specific parameters of the Ca^{2+} response in the different conditions (Figure 2f). In particular, we monitored Ca^{2+} homeostasis, time to egress and peak Ca^{2+} responses. To assess the contribution of PKG to Ca^{2+} homeostasis in intracellular, unstimulated parasites we compared the baseline (basal) Ca^{2+} of WT and Cmpd1 treated cells and observed no difference in GFP/mCherry ratio (Figure 2g); thus, suggesting that cGMP is not linked to modulations of basal Ca^{2+} levels. Next, we assessed the time to egress, which we defined as the time-point that the first parasite exited the confines of the parasitophorous vacuole. WT parasites rapidly egressed in response to all three agonists (Figure 2h–grey bars). In contrast, Cmpd1 treated cells showed defective egress to all stimuli (A23187, BIPPO, and saponin; Figure 2h–purple). To probe the maximal Ca^{2+} responses whilst Cmpd1 inhibited PKG, we performed side-by-side comparison of the peak Ca^{2+} reached after agonist stimulation. BIPPO treatment robustly increases cytoplasmic Ca^{2+} levels of WT cells (Figure 2i–BIPPO, grey bar). In contrast, BIPPO failed to induce comparable peak Ca^{2+} responses when PKG was inhibited (Figure 2i–BIPPO, purple bar), reflecting the visual observations seen in Figure 2ci. This indicates that cGMP signaling acts upstream of Ca^{2+} flux, as PKG activity is required for the cGMP dependent initiation of Ca^{2+} dynamics and egress. In comparison, Cmpd1 treated tachyzoites display Ca^{2+} flux in response to saponin and A23187 stimulation, achieving Ca^{2+} amplification greater than seen in Cmpd1–BIPPO (Figure 2i–saponin, A23187). Importantly, however, these apparently normal peak Ca^{2+} responses were rarely followed by egress when PKG is inhibited with Cmpd1 (Figure 2h, i). This suggests that while Ca^{2+} signaling is essential for egress, and can be stimulated by multiple pathways (here either BIPPO or saponin), it still requires PKG to activate motility. Overall, this work has provided new insights into the hierarchical nature of signal transduction suggesting that cGMP precede Ca^{2+} signaling during activation of egress and motility.

2.3 | *Tg*CDPK3 is not involved in steady state or amplification rate of Ca^{2+} during *Toxoplasma* egress

Previously, it has been shown that *Tg*CDPK3 is important for A23187-induced egress but the role of *Tg*CDPK3 can be bypassed by changes in [K^+] or activation of cGMP signaling (McCoy et al., 2012; Lourido et al., 2012). Whilst *Tg*CDPK3 could be considered an effector of Ca^{2+} signaling, published work suggests that it might act in Ca^{2+} homeostasis or contribute to Ca^{2+} amplification in egress (McCoy et al., 2012; Garrison et al., 2012). To investigate the influence of *Tg*CDPK3 on Ca^{2+}, we introduced GCaMP6s/mCherry into Δ*Tg*CDPK3 tachyzoites. When treated with A23187, Δ*Tg*CDPK3, parasites responded with a uniform increase in cytoplasmic Ca^{2+} but did not reliably egress, in line with previously published work (Lourido et al., 2012; Garrison et al., 2012; McCoy et al., 2012; Figure 3ai) (Movie S7). Ratiometric analysis illustrates the initial peak in Ca^{2+} signal followed by a return to approximate basal levels over the 10 min filming period (Figure 3aii). Activation of cGMP with BIPPO induced a rapid Ca^{2+} amplification and here egress was seen in all tachyzoites tested (Figure 3bi, ii) (Movie S8). Similarly, saponin treatment induced a Ca^{2+} increase followed by egress (Figure 3ci, ii) (Movie S9). To test whether *Tg*CDPK3 is required to maintain basal Ca^{2+} levels as suggested by Garrison *et al.* (2012) (Garrison et al., 2012), we compared the basal Ca^{2+} levels of resting, intracellular Δ*Tg*CDPK3 tachyzoites to WT. Here, we saw no difference between Δ*Tg*CDPK3 and WT lines suggesting no role for *Tg*CDPK3 in Ca^{2+} homeostasis (Figure 3e). Further, when Ca^{2+} potential was probed via measurement of peak Ca^{2+} levels after stimulation, Δ*Tg*CDPK3 tachyzoites were able to upregulate Ca^{2+} to the same extent as WT cells, approximately twofold to fourfold increase (Figure 3f). McCoy *et al.* (2012) hypothesised that *Tg*CDPK3 could be involved in Ca^{2+} amplification by modulating the rate of Ca^{2+} release (McCoy et al., 2012). We therefore measured the rate of change of Ca^{2+} during the amplification stage (Figure 3g–ΔCa^{2+}/s). Between WT and Δ*Tg*CDPK3 tachyzoites, we did not detect a difference in BIPPO and saponin induced Ca^{2+} amplification rates (Figure 3h–BIPPO, saponin). A23187 stimulation saw Ca^{2+} amplification rates of Δ*Tg*CDPK3 only marginally slower than WT (Figure 3h–A23187) suggesting that Δ*Tg*CDPK3

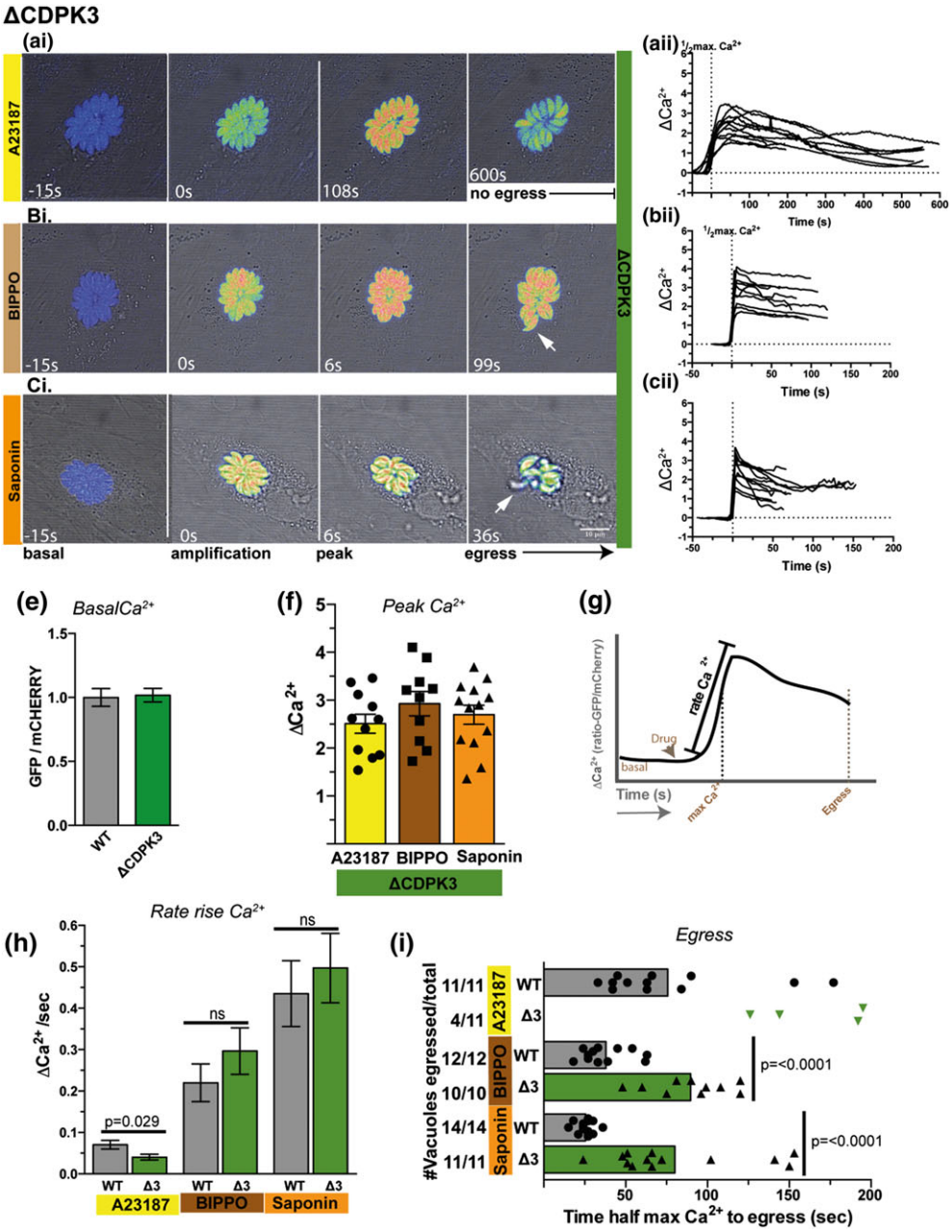

FIGURE 3 Δ*Tg*CDPK3 egress defects can be overcome with activation of cGMP pathways. (ai) Temporal analysis of egress and Ca^{2+} signaling in Δ*Tg*CDPK3 parasites shows A23187 induces Ca^{2+} amplification but not egress. (aii) Ratiometric tracking of Ca^{2+} response demonstrates Ca^{2+} peak prior to slow decline of Ca^{2+} levels over 10 min of filming, parasites do not egress. *n* = 11 vacuoles. (b) Visual (i) and ratiometric (ii) tracking of BIPPO induced Ca^{2+} induction leading to egress of Δ*Tg*CDPK3. *n* = 10 vacuoles. (c) Visual (i) and ratiometric (ii) tracking of saponin induced Ca^{2+} induction leading to egress of Δ*Tg*CDPK3. *n* = 11 vacuoles. (e) Comparison of basal Ca^{2+} of resting intracellular tachyzoites shows no difference between WT v. Δ*Tg*CDPK3 indicating no role for *Tg*CDPK3 in Ca^{2+} homeostasis. (f) Quantitation of Peak Ca^{2+} in Δ*Tg*CDPK3 when stimulated with A23187, BIPPO or saponin show comparable peak Ca^{2+} levels of approximately threefold change indicating no role of *Tg*CDPK3 in Ca^{2+} release potentials. (g) Schematic outlining assessment of rate of change of Ca^{2+} during amplification period. (h) Comparison of WT and Δ*Tg*CDPK3 amplification capacity in response to A23187, BIPPO and saponin. A moderate amplification defect is seen in Δ*Tg*CDPK3 stimulated with A23187; $p = 0.029$, unpaired student t-test −/+ s.e.m. Amplification rates are comparable between WT and Δ*Tg*CDPK3 for BIPPO and saponin treatment. (i) Egress analysis confirms activation of BIPPO and saponin treated Δ*Tg*CDPK3 cells, but not with A23187. BIPPO and saponin egress is significantly delayed in comparison to WT lines ($p < 0.0001$, unpaired student t-test). *n* = 10–14 vacuoles, −/+ s.e.m

largely does not affect the strength or rate in which A23187 induced Ca^{2+} flux occurs. We then monitored time to egress of Δ*Tg*CDPK3 and noticed that despite there being no difference in intracellular Ca^{2+} levels in response to a stimulus, these parasites still had significant delays in egress. From this data, we can surmise that *Tg*CDPK3 does not have a role in basal Ca^{2+} levels or rate of response to an egress stimuli. Furthermore, our data suggests that whilst stimulation of cGMP can overcome the loss of *Tg*CDPK3, it still results in retarded activation of egress and motility, suggesting that this kinase activates another unknown process that is required for rapid egress.

2.4 | *Tg*CDPK1 acts downstream of Ca^{2+} to activate *Toxoplasma* egress

Previously, it has been demonstrated that *Tg*CDPK1 plays a pivotal role in microneme secretion, egress, invasion, and motility. Lourido *et al.* (2010) showed *Tg*CDPK1 knock down lines fail to respond to A23187 egress stimulation demonstrating a block in Ca^{2+} signal transduction (Lourido et al., 2010). To investigate further, the role of *Tg*CDPK1 in the Ca^{2+} signaling hierarchy, we used the ATP analogue, 3MB-PP1, which specifically targets *Tg*CDPK1$_{WT}$ during egress and motility (Lourido et al., 2010). To create a control, a 3MB-PP1-refractory line was made where the *Tg*CDPK1 gatekeeper amino acid was modified from glycine to methionine (*Tg*CDPK1$_{M;}$ Lourido et al., 2010). 3MB-PP1 inhibition of *Tg*CDPK1$_{WT}$ did not alter the Ca^{2+} amplification dynamics when parasites were stimulated to egress with A23187 (Figure 4a–Amplification, Ci) and, as expected, inhibition of *Tg*CDPK1$_{WT}$ prevented egress (Figure 4a–no egress) (Movie S10). It is important to note that, in these circumstances, egress was scored at the point at which the first egressing parasite breached the parasitophorous vacuole. While A23187 induced egress was scored for over half the 3MB-PP1 treated tachyzoites, this egress was clearly defective as the majority of parasites were unable to disseminate away from the parasitophorous vacuole following vacuole breach. A similar response was seen when 3MB-PP1 treated parasites were stimulated with BIPPO where cytoplasmic Ca^{2+} rapidly increased (Figure 4b–amplification, peak, 4Cii) followed by parasitophorous vacuole breach (Figure 4b–*egress, arrows) (Movie S11). Parasites could not successfully engage motility or disseminate across host cells and were thus incapable of reinvasion. 3MB-PP1 refractory lines (*Tg*CDPK1$_{M}$), demonstrated normal egress, demonstrating the specificity this compound to TgCDPK1 in this experimental setup (Figure 4di–iii). Basal Ca^{2+} showed no differences between 3MB-PP1 treatment of WT and 3MB-PP1 treatment of control line *Tg*CDPK1$_{M}$ (Figure 4e). Ratiometric quantitation of peak Ca^{2+} responses confirmed visual observations where *Tg*CDPK1$_{WT}$ inhibition did not alter peak Ca^{2+} ratios (Figure 4f). When 3MB-PP1-treated tachyzoites were able to breach the parasitophorous vacuole, this event was delayed in comparison to normal egress (Figure 4g). Given that loss of *Tg*CDPK1 cannot be rescued by cGMP pathway induction nor saponin, this data provides further validation of differential roles between *Tg*CDPK1 and *Tg*CDPK3 and reinforces the pivotal role of *Tg*CDPK1 as an essential effector of Ca^{2+} signal transduction during egress.

2.5 | *Tg*CDPK1 and *Tg*CDPK3 contribute to Ca^{2+} dynamics immediately prior to egress

It is still not understood how CDPKs function to promote egress and motility. Previous data has suggested that both *Tg*CDPK1 and *Tg*CDPK3 function in controlling microneme secretion (Lourido et al., 2010; McCoy et al., 2012; Lourido et al., 2012), but whether *Tg*CDPK1 and *Tg*CDPK3 act directly to promote secretion of these organelles or whether they work in an upstream signaling event is unknown. During analysis of CDPK mutants, we noticed differences in the decay of the Ca^{2+} response from peak level to egress. We found that after stimulation of egress, intracellular Ca^{2+} rose to peak levels, and then, decreased (~25%) before egress begun, suggesting that there may be feedback mechanisms to quench Ca^{2+} flux required for egress to proceed. To analyse if CDPKs could be involved in the Ca^{2+} decay, and thus potentially explain a function of these kinases, we probed the kinetics of Ca^{2+} decay during the period between peak Ca^{2+} and egress. Saponin was used to assay this as it activates egress in the absence of continued pharmacological pressure (as is the case with A23187 or BIPPO). For further dissection of peak to egress Ca^{2+} kinetics, traces were averaged, normalized to peak ratio (0) and analysed as a two-step response (Figure 5a–two phase split at ½ Ca^{2+} decay between peak and egress). Where *Tg*CDPK1 is inhibited with 3MB-PP1, and in control *Tg*CDPK1$_{M}$ lines, the point when the ½ Ca^{2+} decay was reached was around 10 s post peak ratio with continuation of Ca^{2+} decay rate until egress at around 25 s post peak ratio. In 3MB-PP1 treated or Δ*Tg*CDPK3, the halfway point (½ Ca^{2+} decay) was slightly delayed to between 15 and 20 s (Figure 5b, inset). Here, the rate of decay for 3MB-PP1 treated or Δ*Tg*CDPK3 shows a distinct change slowing between halfway Ca^{2+} decay to egress. For comparison, we generated a GCaMP6s line where microneme protein Perforin-Like Protein 1 was knocked out (Δ*Tg*PLP1), which causes egress defects due to the inability of parasites to enzymatically breakdown membranes during escape of parasitophorous vacuoles (Kafsack et al., 2009). Our analysis revealed normal intracellular Ca^{2+} signaling in Δ*Tg*PLP1 egress, with peak and Ca^{2+} amplification comparable to WT (Supp. Figure 2a-c) (Movie S12, 13). As expected, Δ*Tg*PLP1 egress was defective in response to A23187; however, Δ*Tg*PLP1 parasites exhibited delayed egress to BIPPO and saponin treatment, most likely due to other means of membrane destruction (Supp. Figure 2ciii). When peak to egress Ca^{2+} decay was quantitated for Δ*Tg*PLP1 decay displays continual rate across the two phases, in contrast to the changes observed upon 3MB-PP1 treatment or *Tg*CDPK3 deletion.

When quantitated as a rate of decay (ΔCa^{2+}/s) from Ca^{2+} peak to ½ ΔCa^{2+} decay (first half decay), there were comparable rates between all conditions including 3MB-PP1 and Δ*Tg*CDPK3 (Figure 5c). In comparison, analysis of the second half of Ca^{2+} dampening before egress (Ca^{2+} decay halfway to egress) demonstrated a specific and statistically significant defect where either *Tg*CDPK1 or *Tg*CDPK3 were defective (approx. −0.01 ΔCa^{2+}/s) as compared to WT or *Tg*CDPK1$_{M}$ (approx. −0.06 ΔCa^{2+}/s), or Δ*Tg*PLP1 (approx. −0.04 ΔCa^{2+}/s; Figure 5c). Overall, our data shows modified Ca^{2+} decay specific to *Tg*CDPK1 and *Tg*CDPK3 suggesting these kinases play roles in modulating Ca^{2+} levels prior to egress and suggest a possible mechanism by which these kinases work to regulate motility during cell exit.

2.6 | cGMP and Ca^{2+} signaling are interconnected during *Toxoplasma* motility

Upon egress, extracellular tachyzoites require gliding motility for movement across the extracellular substrate. We sought to understand the Ca^{2+} signaling dynamics during motility through observations of Ca^{2+} flux using our GCaMP6s approach. Tachyzoites were freshly harvested in Ringer's medium (with Ca^{2+}) and allowed to settle on a substrate surface, before stimulation with motility agonists for a total analysis time of 4 min (2 min prestimulation, 2 min poststimulation). Prestimulation, the majority of tachyzoites exhibit low motility and

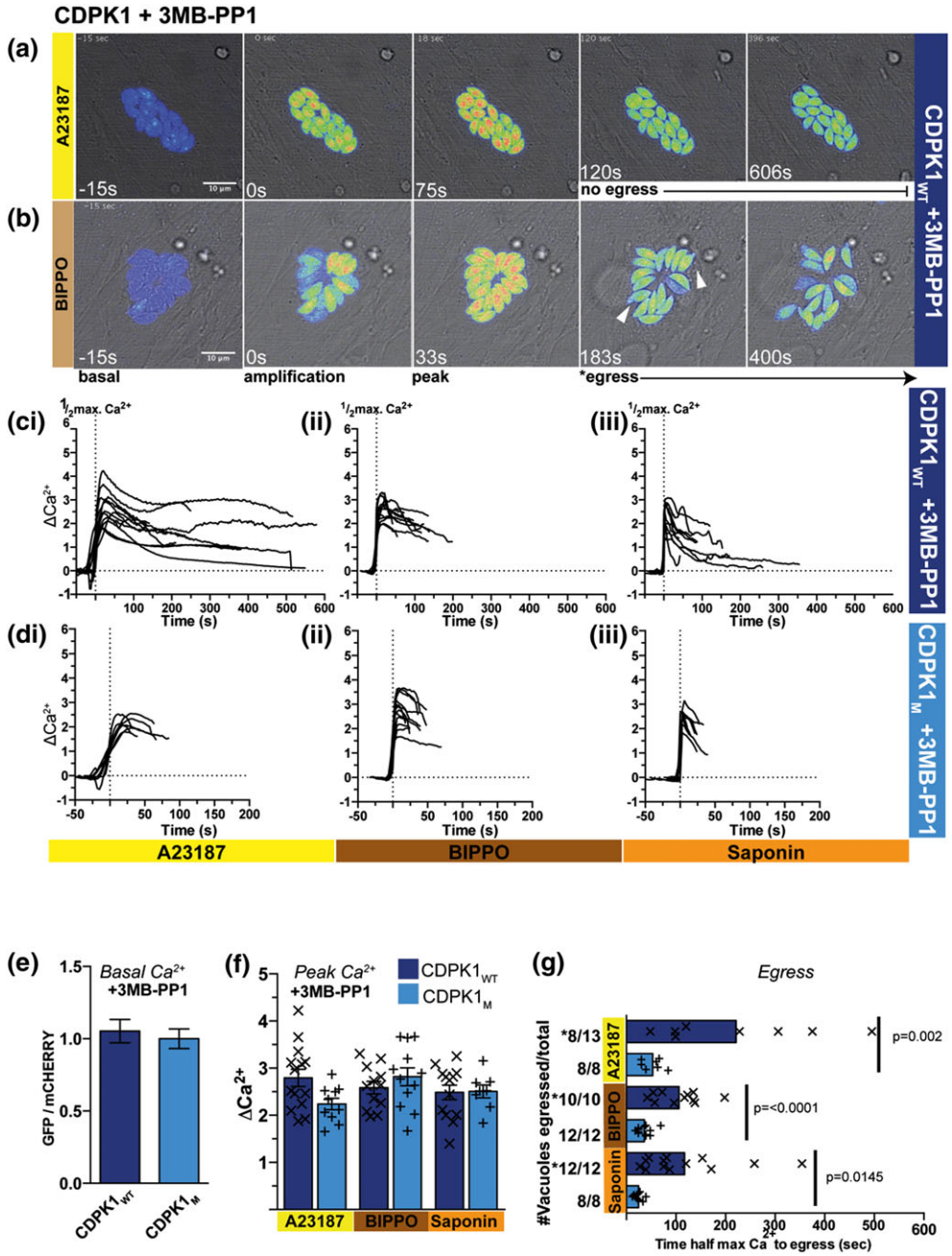

FIGURE 4 *Tg*CDPK1 is required downstream of Ca^{2+} signaling during *Toxoplasma* egress, (a) Temporal analysis of 3MB-PP1-treated tachyzoites shows intact Ca^{2+} responses to A23187 stimulation but egress does not occur within a 10 min timeframe. (b) BIPPO induction of Ca^{2+} signaling for 3MB-PP1 pretreated parasites. Tachyzoites do engage with parasitophorous membranes (arrows) although do not disseminate away from vacuoles productively. First instances of parasite interaction with parasitophorous membranes is scored as faulty egress (*egress). (c) Ratiometric tracking of Ca^{2+} dynamics shows normal amplification and peak Ca^{2+} of 3MB-PP1 treated lines for stimulation with A23187 (i), BIPPO (ii), and saponin (iii) n = 8–13 vacuoles. (d) A point mutation of the gatekeeper residue at the opening of the nucleotide-binding pocket (Gly to Met) renders *Tg*CDPK1$_M$ resistant to 3MB-PP1 inhibition. *Tg*CDPK1$_M$ parasites pretreated with 3MB-PP1 respond to A23187 (i), BIPPO (ii) and saponin (iii) similar to WT showing no obvious defects in Ca^{2+} or egress responses. (e) Intracellular Ca^{2+} ratios are comparable between 3MB-PP1 sensitive and resistant (*Tg*CDPK1$_M$) lines, assessed as GCaMP6s/mCherry ratio, measured over 15 s, normalized to 1 = CDPK1$_M$ + 3MB-PP1 average. (f) Both 3MB-PP1 sensitive and resistant (*Tg*CDPK1$_M$) lines induced similar Ca^{2+} peak ratios prior to *egress for A23187, BIPPO and saponin stimulation. (g) Egress was morphologically abnormal and delayed in all 3MB-PP1 sensitive *egress stimulations. *Tg*CDPK1$_M$ 3MB-PP1 resistance retains normal kinetics with egress occurring within 100 s for all conditions. −/+s.e.m. unpaired student t-test

low Ca^{2+} (Figure 6ai, bi) (Movie S14, 15). Where parasites do engage motility, there is a coincident increase in Ca^{2+} activity (Figure 6ai, bi arrows). To validate the detection of Ca^{2+} signaling in our model, we first stimulated these cells with A23187 and detected a rapid increase in tachyzoite movement and Ca^{2+} signaling (Figure 6aii, representative 60 s time-lapse) (Movie S14). Next, to assess the participation of cGMP signaling in motility tachyzoites were stimulated with BIPPO. Similar to egress, tachyzoites rapidly engaged Ca^{2+} signaling and initiated gliding motility in response to BIPPO, indicating a role for cGMP in signaling for movement (Figure 6bii, representative 60 s time-lapse)

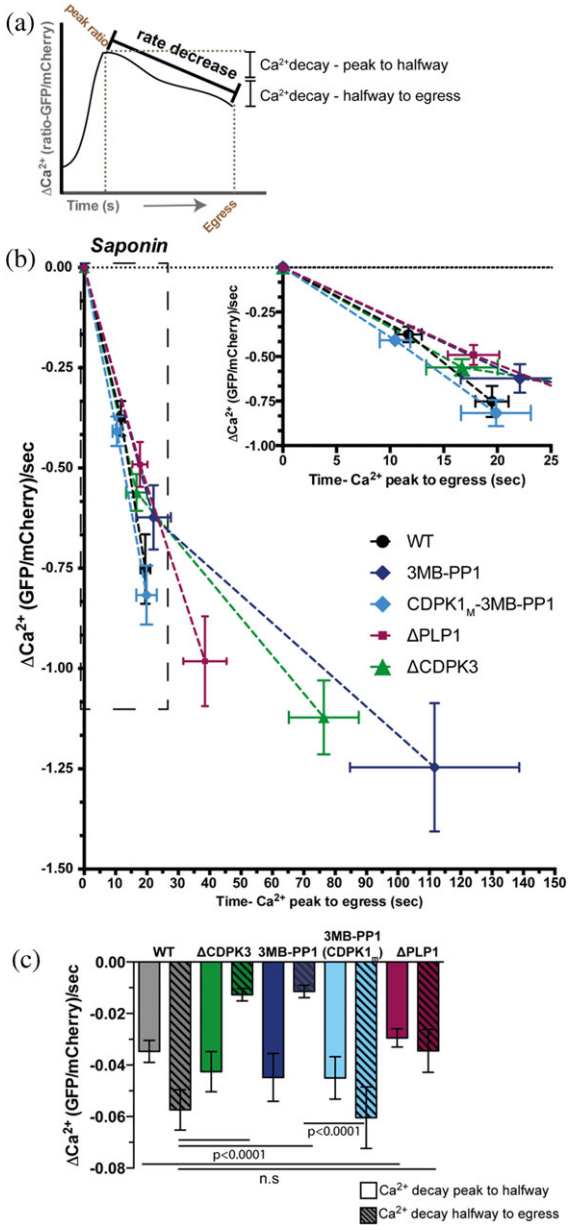

FIGURE 5 *Tg*CDPK1 and *Tg*CDPK3 play a role in Ca^{2+} dampening prior to egress, (a) Schematic outlining ratiometric analysis of Ca^{2+} sequestration immediately prior to egress, denoted as rate decrease. Analysis was performed in two phases; Ca^{2+} decay peak to halfway and Ca^{2+} decay halfway to egress. Halfway is defined as point at which ΔCa^{2+} is 50% of $Ca^{2+}{}_{peak}$–$Ca^{2+}{}_{egress}$. (b) Analysis of saponin-treatment traces reveals differences between WT (black), Δ*Tg*CDPK3 (green) and 3MB-PP1 (blue) treated tachyzoites in the peak to egress phase. Rate of decrease was assessed with Peak Ca^{2+} normalized to 0. Kinetics of Ca^{2+} sequestration in the peak to halfway phase shows similar rates of Ca^{2+} decrease in all cell lines (inset). Halfway to egress analysis shows a dramatic decrease in Ca^{2+} decay and delay to initiation of egress for Δ*Tg*CDPK3 and 3MB-PP1 treated WT tachyzoites (light blue). Deletion of microneme protein *Tg*PLP1 causes delayed saponin induced egress with a Ca^{2+} decay rate distinct from that of CDPK mutants. (c) Quantitation of Ca^{2+} rate decrease shows comparable rates between all lines for peak to halfway Ca^{2+} decay phase. WT lines maintain the rate of decay in the hallway to egress phase. Δ*Tg*CDPK3 and 3MB-PP1 biphasic response shows clear, significant decreases in Ca^{2+} decay rate in the halfway to egress phase that is no present in WT, $CDPK1_M$ or egress defective Δ*Tg*PLP tachyzoites. Student *t*-test −/+ s.e.m. n = 7–13 vacuoles

(Movie S15). During motility, parasites display multiple forms of movement defined as productive; helical (corkscrew-like motion) and circular, or unproductive; twirling and short movements. Quantitation of motility between A23187 and BIPPO showed both compounds induced all forms of movement at comparable levels, with around 70% of tachyzoites exhibiting some form of movement (Figure 6c, WT–A23187 vs. BIPPO). To analyse further the role of cGMP signaling in motility we pretreated tachyzoites with Cmpd1, inhibiting PKG, before activation with BIPPO. Here, we saw only a small proportion of tachyzoites engage motility, predominantly with nonproductive twirling or short movements. To examine the link between Ca^{2+} flux and movement seen in our visual data (Figure 6a,b), and to assess the contribution of cGMP signal disruption in Cmpd1 defective motility, we quantitated the tachyzoite population average of the Ca^{2+} signal during motility assays. Prior to stimulation, WT populations maintained a stable 'basal' Ca^{2+} profile, which rapidly increased upon the addition of agonists A23187 and BIPPO, coincident with movement (Figure 6d, A23187–Black line, BIPPO–Brown line). In contrast, Cmpd1 pretreated cells displayed a lowered basal Ca^{2+} level with minimal increases after A23187 or BIPPO stimulation (Figure 6d Cmpd1, A23187–Blue line, BIPPO–Purple line). This demonstrates that, like signaling pathways in egress (Figure 2), cGMP signaling through PKG is an important signaling module driving tachyzoite movement.

2.7 | Level of Ca^{2+} signaling correlates with the quality of motility in *Toxoplasma*

Apicomplexan motility can often alternate between bursts of movement and inertness (Münter et al., 2009; Williams et al., 2015). To determine if modulation of cytoplasmic Ca^{2+} levels was responsible for these motility bursts, we tracked the displacement and Ca^{2+} flux of individual tachyzoites. We followed productively motile tachyzoites engaged in circular or helical movement after drug stimulation and compared these with parasites that remained nonmotile throughout the assay. Prior to stimulation parasites were nonmotile travelling no more than 1 μm at a time (Figure 7a, b–thin black lines). During this nonmotile period Ca^{2+} flux remained consistently low (Figure 7a, b–thick grey lines). Upon stimulation with A23187, helical movement drove bursts of increased displacement with tachyzoites travelling up to 5 μm at a time (Figure 7ai–thin black line). Here, dynamic Ca^{2+} flux (rapid, high amplitude Ca^{2+} transients) paralleled tachyzoite movement during circular movements. In the case of the individual tachyzoite plotted, two circular revolutions were completed before a switch to twirling motility (Figure 7ai thick lines–gold = circle 1, pink = circle 2, and twirling = blue). Displacement versus Ca^{2+} level showed a moderate correlation of r^2 = 0.6703 (Figure 7ai, right plot—correlation quantitation taken from data highlighted in grey). A similar moderate correlation between displacement and Ca^{2+} was seen for helical motility where Ca^{2+} flux mirrored parasite displacement in bursts of activity (Figure 7aii–maroon–helical). In contrast nonmotile parasites, by definition, did not travel more than 1 μm at a time, and although Ca^{2+} release was evident with a slight increase in the Ca^{2+} signal, dynamic Ca^{2+} flux was not seen and did not correlate with displacement 7. This indicates that dynamic and higher amplitude Ca^{2+} fluxes are important for motility and lower amplitude and sustained rises in

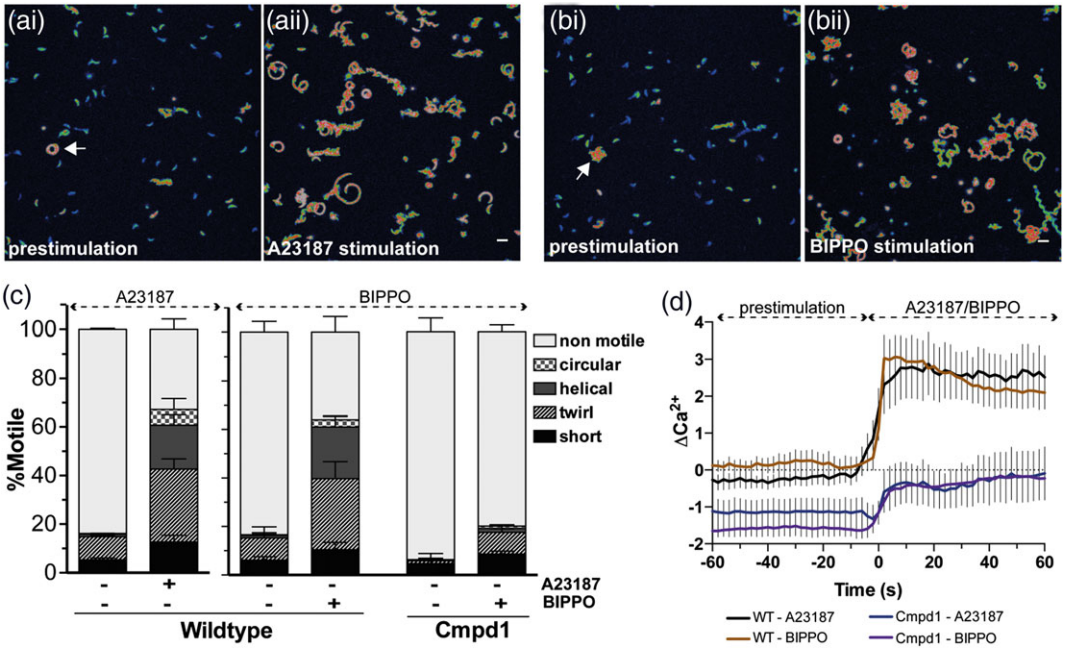

FIGURE 6 cGMP and Ca^{2+} signaling are interconnected during *Toxoplasma* motility. (ai, bi) Extracellular tachyzoites settled onto substrate maintain low Ca^{2+} and low motility prestimulation, time-lapse projection over 60 s. False colored Ca^{2+} reads; blue = low Ca^{2+}, red = high Ca^{2+}. Where parasites are motile in these conditions Ca^{2+} signaling is also evident (arrows). A23187 (aii) or BIPPO (bii) activates Ca^{2+} signaling and motility in extracellular tachyzoites, time lapse projection over 60 s. (c) Tachyzoite movement classification where >80% of WT parasite are nonmotile prestimulation but show ~80% induction of either circular, helical, twirling or short motility after A23187 or BIPPO stimulation. Cmpd1 pretreatment prevents motility activation with ~80% of parasites remaining nonmotile after BIPPO stimulation. (d) Population averages of Ca^{2+} responses over time demonstrate gross Ca^{2+} induction of the entire population. Cmpd1 inhibition sees tachyzoite populations maintain a lower resting GCaMP6s/mCherry ratio that fails to induce robust Ca^{2+} changes after A23187 or BIPPO activation (purple line). Normalised average WT GFP/mCherry over an unstimulated 60 s period. WT; n = 6, Cmpd1; n = 5, −/+s.e.m

cytoplasmic Ca^{2+} were not sufficient to drive motility. Assessment of BIPPO induced motility showed similar results to A23187 treatment, with dynamic Ca^{2+} flux moderately correlated with displacement in circular and helical movement but not in nonmotile parasites (Figure 7 bi–iii). Quantitative comparison of the motility parameters demonstrated the average parasite velocity of 1–1.5 μm/s for both helical and circular motility in response to A23187 or BIPPO (Figure 7ci). Parasites travelled an average of 8 μm over an average of 8 s between Ca^{2+} peaks in helical movement (Figure 7cii, iii–helical). In response to BIPPO treatment, parasites travelled slightly further (~12 μm) over a longer Ca^{2+} flux period (~11 s) when engaged in circular motility (Figure 7cii, iii–circular). To scrutinize further the dynamics in nonmotile parasites, we examined the Ca^{2+} profiles of nonmotile cells pretreated with Cmpd1. Similar to WT, a slight rise in Ca^{2+} was seen but neither correlation nor significant Ca^{2+} flux was evident in response to either A23187 or BIPPO stimulation (Figure 7di, ii). Here, we see that Ca^{2+} flux did not occur in the absence of PKG activity outlining a similar signaling hierarchy between motility and egress where cGMP precedes Ca^{2+}.

3 | DISCUSSION

In this work, we investigate the interactions between signal transduction pathways that drive egress and motility in *Toxoplasma*. Using the Ca^{2+} biosensor GCaMP6s, we confirm and extend previous work on Ca^{2+} signaling in *Toxoplasma* and other apicomplexan parasites (Lovett, 2003; Brochet et al., 2014; Carey et al., 2014; Brown et al., 2016; Sidik et al., 2016). Key parameters of cytosolic Ca^{2+} fluxes, such as signal amplitude, frequency and decay were monitored, which in other systems can determine the type of cellular response that is invoked by these signaling events. Furthermore, we use specific inhibitors and activators as well as several mutants known to play a role in Ca^{2+} signaling to determine the hierarchy of events that take place that ultimately leads to egress and motility—a key event in the pathogenicity of all apicomplexan parasites.

Our work suggests that cGMP and the activity of PKG acts upstream of Ca^{2+} release to activate *Toxoplasma* motility. This work builds on recent findings in *P. berghei* ookinetes where Brochet *et al.* (2014) identified a potential link between cGMP and Ca^{2+} signal transduction (Brochet et al., 2014). In this study, they identify PKG-dependent phosphorylation of components involved in phosphoinositide metabolism, a pathway that in mammalian systems leads to the production of the second messenger IP_3, which in turn activates Ca^{2+} release channels at the ER (Berridge et al., 2003). Furthermore, two very recent studies have shown that cGMP and Ca^{2+} signaling are also linked in *Toxoplasma*. In this regard, our work corroborates these similar findings but uses the more potent apicomplexan-specific PDE inhibitor BIPPO (Howard et al., 2015). Overall, this combined work now strongly supports a mechanism where Ca^{2+} and cGMP pathways are linked across apicomplexan species.

This work also highlights the complexities and redundancies of signal transduction networks in apicomplexan species. We show that a rise in intracellular Ca^{2+}, but not egress, can occur independently of

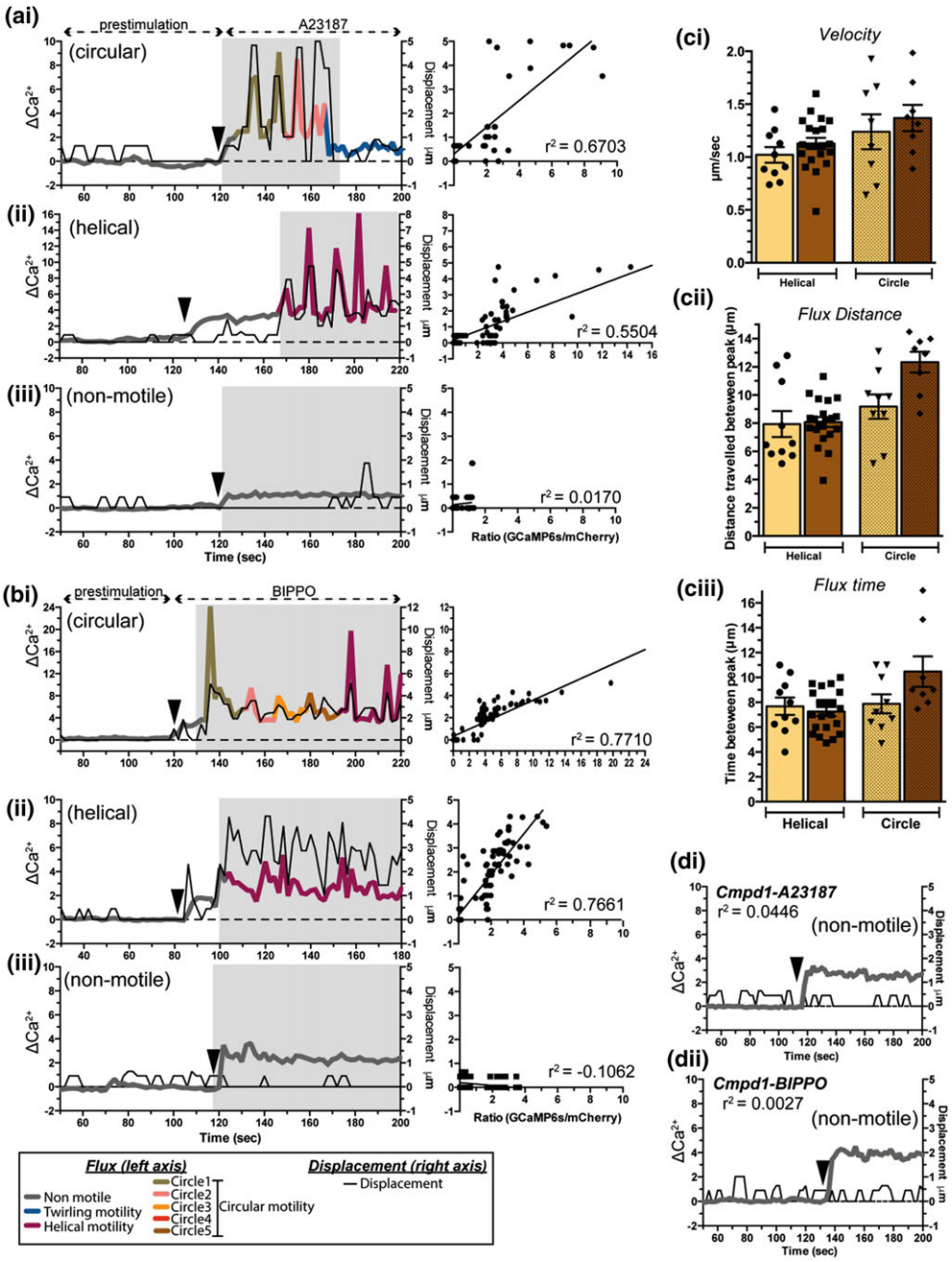

FIGURE 7 Level of Ca^{2+} signaling correlates with the quality of motility in *Toxoplasma*, Individual motility profiles tracking parasites in response to A23187 (a) and BIPPO (b) stimulation. In all cases, prior to stimulation displacement remains <1 µm (nonmotile = thick grey line, µm = thin black line). Circular (ai, bi) and helical (aii, bii) motility show a moderate correlation between displacement and Ca^{2+} flux where bursts of motility are paralleled with Ca^{2+} peaks (circles = colored lines, helical = maroon, twirling = blue). Parasites that remain nonmotile poststimulation do not show dynamic Ca^{2+} flux or correlation between Ca^{2+} and displacement (aiii, biii; Greyed out zone represents data incorporated into correlation assessment). Quantitation of motility parameters velocity (ci), flux distance–distance travelled between Ca^{2+} peaks (cii), and time elapsed between Ca^{2+} peaks (ciii). *n* = 8–20 individual parasites tracked for each condition, displayed as points, −/+ s.e.m. (di, ii) Cmpd1 pretreated parasites are not motile and do not display Ca^{2+} flux when activated with A23187 or BIPPO

cGMP signaling through *Tg*PKG. This is demonstrated by altering host cell and vacuolar milieus (i.e., $[K^+]$ and pH levels) with saponin treatment showing that this causes a rapid induction of Ca^{2+} signaling independent of *Tg*PKG activity. This suggests the presence of redundant mechanism(s) complementary to the cGMP/PKG activation that can also feed into a rise in Ca^{2+} signaling for subsequent motility and egress. One such candidate for alternate activation of Ca^{2+} signaling is cAMP, which we show is produced when BIPPO is administered. Other possibilities include cADPR signal transduction pathway (Chini, Nagamune, Wetzel, & Sibley, 2005) and Abscisic Acid driven pathways (Nagamune et al., 2008). However, there is little understood about these pathways and no specific genes nor inhibitors are known, so assessing their interaction with Ca^{2+} signaling is currently challenging. What is clear, as presented in this study and in support of the current literature, is that intracellular tachyzoites can sense and respond to multiple stimuli (Moudy, Manning, & Beckers, 2001; Persson et al.,

2007; Niedelman, Sprokholt, Clough, Frickel, & Saeij, 2013; Roiko et al., 2014; Borges-Pereira et al., 2015). What is unclear, is the identity of physiological stimulators of egress and motility. Brown *et al.* recently shown that serum albumin can stimulate microneme secretion in a Ca^{2+} independent fashion but no other natural triggers are known (Brown et al., 2016).

In other systems, mechanisms of cytosolic Ca^{2+} concentration are controlled by Ca^{2+} pumps and channels, which in turn alter the frequency, location and amplitude of Ca^{2+} transients to drive distinct biological functions (Berridge et al., 2003). Here, we identified amplification and dampening Ca^{2+} dynamics in *Toxoplasma* where, prior to egress cytoplasmic Ca^{2+} release is followed by a ~ 20 s period of Ca^{2+} decay. This data showed that while *Tg*CDPK1 and *Tg*CDPK3 are not required for Ca^{2+} peak levels, their attenuation slowed Ca^{2+} decay immediately prior to egress. Whilst the importance or function of this Ca^{2+} dampening is unknown the fact that *Tg*CDPK1 or *Tg*CDPK3 mutants show this Ca^{2+} attenuation, and do not egress efficiently, suggests that these kinases may hold some important role during this process. What is clear from this analysis is that Ca^{2+} fluctuations are dynamic and must require mechanisms for both Ca^{2+} release and re-uptake into an internal store or efflux to the extracellular environment. In *Toxoplasma*, a thapsigargin-sensitive sarcoplasmic-ER Ca^{2+} ATPase (SERCA) is present at the ER while a Ca^{2+}/H^{+}-ATPase (*Tg*A1) at the acidocalcisome is required for Ca^{2+} homeostasis (Luo, Ruiz, & Moreno, 2004; Nagamune, Beatty, & Sibley, 2007). However to date, the identity and regulation of Ca^{2+} release channels, nor the contribution of *Tg*A1 and *Tg*SERCA in egress and motility has not been described.

Our data shows that each Ca^{2+} oscillation is accompanied by approximately 8 μm of tachyzoite movement. Given that *Toxoplasma* tachyzoites are ~7 μm in length this suggests that each Ca^{2+} flux event allows for parasites to move one body length. Similarly, in *P. berghei* sporozoites weak correlations were observed between Ca^{2+} flux and sporozoite speed, although quantitation of distance travelled per Ca^{2+} peaks were not performed (Carey et al., 2014). Indeed, the current model of motility suggests that adhesins released from the micronemes link host substrate to the parasite glideosome and action of the motor pulls adhesins rearward to drive for forward movement (Münter et al., 2009; Heintzelman, 2015). Data presented here therefore suggests that Ca^{2+} flux may induce a wave of adhesins to be secreted from the micronemes onto the surface, which then engage with the glideosome and drive another parasite length of motility before another Ca^{2+} dependent release is required. Indeed, *Toxoplasma* is able to secrete successive rounds of micronemal proteins upon stimulation further adding weight to this hypothesis (Bullen et al., 2016).

Overall, this work aims to incorporate apicomplexan signaling pathways as a unified–albeit complex–network, to produce a hierarchical model of pathway activation from external stimuli to internal signal transduction pathways. Importantly, we have built on work defining a link between cGMP and Ca^{2+} signaling pathways while also detecting potential feedback mechanisms between CDPKs and Ca^{2+}. Further, we show a correlation between Ca^{2+} flux and parasite movement that strengthens the current model for Ca^{2+}-mediated, adhesin-based gliding motility. This work also highlights the utility of biosensor technology in dissecting components of signal transduction and demonstrates the potential of this application for further analysis of Ca^{2+} dynamics in *Toxoplasma*. Of particular interest would be the targeting of biosensors to subcellular domains to identify more subtle, localized instances of signal initiation or transduction.

4 | EXPERIMENTAL PROCEDURES

4.1 | Parasite culture and harvest

Primary human foreskin fibroblasts (HFFs) cells were maintained in culture at 37°C/10% CO_2 with DMEM supplemented with 10% cosmic calf serum. Prior to inoculation, HFFs were refreshed with D1–DMEM supplemented with 1% FCS and 1% Glutamax™ (Invitrogen). Parasites were inoculated onto HFFs and maintained at 37°C/10%CO_2.

4.2 | Generation of transgenic parasites

pGP-CMV-GCaMP6s was a gift from Douglas Kim (Addgene plasmid #40753). For our work GCaMP6s was amplified and Gibson assembled with mCherry, driven by *Tg*TUB1 and *Tg*GRA1 promoters, respectively. Plasmids were transfected for homologous recombination into the *uprt* locus using FUDR selection, which was subsequently confirmed by fluorescent microscopy.

4.3 | Tachyzoite preparation for analysis

4.3.1 | Ca^{2+} source assessment

Fresh tachyzoites were harvested and inoculated onto confluent host cells and grown for 24–30 h in D1. Wells were washed once with PBS before addition of modified Ringer's + EGTA Buffer (155 mM NaCl, 3 mM KCl, 5 mM $MgCl_2$, 3 mM NaH_2PO_4, 10 mM HEPES, 10 mM glucose, and 0.1 mM EGTA; Lovett, 2003). Tachyzoites were harvested prior to vacuole rupture and analysed as per motility (see below).

4.3.2 | Egress

Fresh tachyzoites were harvested and inoculated onto confluent host cells grown on IBIDI tissue culture-treated 8-well chamber slides and allowed to grow for 24–30 h in D1. Ringer's media (155 mM NaCl, 3 mM KCl, 2 mM $CaCl_2$ 1 mM $MgCl_2$, 3 mM NaH_2PO_4, 10 mM HEPES, 10 mM glucose) replaced D1 prior to imaging. Where applicable inhibitor drug treatments (Cmpd1–5 μM, ≥25 min @37°C. 3MB-PP1–5 μM, ≥20 min @37°C) were performed in Ringer's media prior to egress analysis. Imaging was restricted to vacuoles containing 8–16 tachyzoites where host cells were only infected with a single vacuole. Agonist drugs (A23187–4 nM, BIPPO–55 μM, saponin–0.05% *w/v*) were added into chamber via catheter tubing 15 s after initiation of image acquisition. ≥8 vacuoles were analysed for each condition.

4.3.3 | Motility

Fresh tachyzoites were harvested and inoculated onto confluent host cells and grown for 24–30 h in D1. Where applicable wells were pretreated with inhibitors. Wells were washed once with Ringer's media and tachyzoites were harvested prior to vacuole rupture via scraping, needle passing through 27-gauge needle and filtration of cell debris (3 μm filter). IBIDI 8-well chambers slides were pretreated with

Poly-L-Lysine for 20 min at RT and allowed to dry. Free tachyzoites were inoculated onto Poly-L-Lysine surface and allowed to settle for 3 min. Tachyzoite motility was captured for 2 min prior to addition of compounds (A23187 and BIPPO) via catheter tubing for a total of 4 min image acquisition. Assays were performed in duplicate. Parasite movement was scored by eye from acquired videos in with ~100 parasites analysed per repeat, $n = 3$.

4.4 | Imaging platform, acquisition settings and analysis

4.4.1 | Egress

Imaging was performed on the Leica SP8 Confocal system, 63 × /1.4 NA Oil immersion objective, in humidified environmental chamber with temperature maintained at 37°C. Image capture was managed by Leica software with acquisition across 5 × 1.25 µm Z-stacks, 1 frame/3 s until egress was detected or up to a maximum of 10 min. Image analysis was performed using FIJI software with Macros designed by Dr. Lachlan Whitehead specifically for use during this project (available upon request). Fluorescent readout was converted from a visual to digital signal for both mCherry (control) and Ca^{2+} sensitive GCaMP6s signals. Signal was normalized to 0 (zero) GCaMP6s/mCherry ratio at $t = 0$ s on the y-axis using $^1/_2$ Ca^{2+} Max:

$$\frac{(\mathbf{Ratio}_{Peak} - \mathbf{Ratio}_{Basal})}{2}$$

Egress is defined as first instance of parasite movement from the vacuole (pinching through host membrane or movement away from vacuole). Peak Ca^{2+} represents the maximum GCaMP6s/mCherry ratio reached per vacuole (n = 8–13 vacuoles, mean +/− s.e.m.). Rate increase was determined as:

$$\frac{(\mathbf{Ratio}_{Peak} - \mathbf{Ratio}_{Basal})}{\mathbf{t}_{Peak} - \mathbf{t}_{2\%}}$$

where $Ratio_{Peak}$ is the peak GCaMP6s/mCherry ratio per vacuole, $Ratio_{Basal}$ is the GCaMP6s/mCherry ratio averaged across time-points prior to Ca^{2+} induction, t_{Peak} is time peak ratio reached (s) and $t_{2\%}$ is first instance of Ca^{2+} induction above 2% peak Ca^{2+} (s).

For Ca^{2+} decrease from peak analysis plots were normalized so 0 = t_{Peak} (x) and $Ratio_{Peak}$ (y). Vacuole Ca^{2+} traces were averaged. 50% Ca^{2+} decay from peak to egress was plotted as:

$$\frac{\mathbf{Ratio}_{Peak} - \mathbf{Ratio}_{Egress}}{y = \quad 2 \quad x = t \text{ from peak } (s)}$$

100% decay from peak to egress was plotted as:

$$y = \mathbf{Ratio}_{Peak} - \mathbf{Ratio}_{Egress} \qquad x = t \text{ from peak } (s)$$

Rate decay from peak to egress was determined as:

$$1^{st} Half : \frac{\mathbf{Ratio}_{50\%Ca2+decay}}{\mathbf{t}_{50\%Ca2+decay} - \mathbf{t}_{peak}} \quad 2^{nd} Half : \frac{\mathbf{Ratio}_{100\%Ca2+decay} - \mathbf{Ratio}_{50\%Ca2+decay}}{\mathbf{t}_{100\%Ca2+decay} - \mathbf{t}_{50\%Ca2+decay}}$$

4.4.2 | Motility

Imaging was performed as per egress with a 40 ×/ 1.4 NA Oil immersion objective, acquisition across 3 × 1.25 µm in z direction, 1 frame/2 s. Whole population changes were determine using FIJI intensity plot feature and normalized to 0 (zero) GCaMP6s/mCherry ratio where 0 = average of WT population over 60 s of nonstimulated parasite filming. Tracking of individual parasites was performed using FIJI software with Macros designed by Dr. Lachlan Whitehead specifically for motility and Ca^{2+} tracking during motility within this project–adapted from TrackMate plugin. Data was processed in Excel. Types of movement for individual parasites were scored by eye and aligned with ratiometric readouts. For each parasite, Ca^{2+} was internally normalized to zero based on the average of a period of immobility extended across 60 s. Parasites were selected for individual tracking if they displayed predominant helical or circular movement, were in frame for both nonmotile and motile periods and did not cross paths with other tachyzoites. Representative plots shown are derived from independent experiments, n = 5–8.

4.4.3 | Motility parameters

Ca^{2+} and displacement traces from above were analysed to determine velocity: total distance travelled (µm)/time (s); Flux distance: average distance travelled for each Ca^{2+} peak in an individual parasite, one point = one parasite track (multiple Ca^{2+} peaks); Time between peaks: average time between each Ca^{2+} peak for an individual parasite, one point = one parasite track (multiple Ca^{2+} peaks). n = 8–20 parasites for each condition and movement type.

4.5 | Compound synthesis

Compound 1 and 3MBP-PP1 were prepared according to literature procedures (Biftu et al., 2005; Lourido et al., 2010; Towle, Chang, Kerns, & Bhanot, 2013).

4.6 | LC–MS analysis of cyclic nucleotide levels

Intracellular tachyzoites were recovered from host cells by needle passage and filtering through a 0.45 µm membrane. Purified tachyzoites (3×10^8) were resuspended in DME supplemented with 10 mM HEPES pH 7.2, prior to the addition of either BIPPO (1 µM) or A23187 (2 µM). Tachyzoite suspensions were incubated for 1 min in a 37°C water bath, then rapidly transferred to ice cold PBS to quench metabolism and centrifuged (20,000 rpm, 5 min). Tachyzoite cell pellets were extracted in 10-volumes of ice cold acetonitrile containing 2 µM ^{13}C,^{15}N–AMP and ^{13}C,^{15}N–UMP and extracts vortex mixed (1 min), then sonicated in an ice-water bath (5 min), before centrifugation (20,000 rpm, 10 min, 4°C). The supernatants were transferred into HPLC vials, and cyclic nucleotides detected using LC-QTOF as previously described Hortle et al., 2016 with the following modifications (Hortle *et al*., 2016). LC analysis was performed on an Agilent 1260 HPLC system using a ZIC®-pHILIC column 5 µm particle size, 150 × 4.6 mm, Merck SeQuant®), a 23 minute gradient (containing a 6 min washout and equilibration) with mobile phases A (20 mM ammonium carbonate pH 9) and B (100% acetonitrile) eluted at a constant flow rate of 300 µL/min (25°C) and a sample injection of 5 µL. MS was performed on an Agilent 6545 QTOF instrument and ionization promoted with a capillary voltage of 2.5 kV, drying gas flow of 10.0 L/min (N_2) and temperature of 225°C, nebulizer pressure of

20 psi, fragmentor and skimmer cap voltage of −125 V and −45 V, respectively. Ions were analysed in negative mode with a full scan range of 85 to 1200 m/z at a rate of 0.8 spectra/sec and peaks identified using MassHunter Quantitative Analysis B.07.00 (Agilent). Metabolite identification of purines of interest (ATP, GTP, and cAMP) was based on accurate mass, predicted retention time and authentic chemical standards (level 1 standard of identification according to the Metabolomics Standards Initiative). cGMP was identified based on accurate mass and predicted retention time (level 2 standard of identification). All samples were randomized prior to analysis and pooled biological quality control samples (pbQCs) were prepared by pooling 10 µl of all samples lysate and run every five samples to monitor instrument reproducibility.

ACKNOWLEDGMENTS

We would like to thank Professor Silvia N.J Moreno, University of Georgia, USA for useful and generous discussions and Professor Vern Carruthers for sharing the ΔPLP1 line. We also thank C. Bradin for assistance in construct preparation.

RJS is supported by an Australian Postgraduate Award and CJT by a an Australian Research Council (ARC) Future Fellowship. MJM is an NHMRC Principal Research Fellow. This work was supported by NHMRC project grants GNT1022559, GNT1047806 and GNT1017059 and institutional support from the Victorian State Government Operational Infrastructure Support, the Australian Cancer Research Foundation and the Australian Government NHMRC IRIISS. The funders had no role in study design, data collection and analysis, decision to publish, or preparation of the manuscript.

COMPETING INTERESTS

The authors declare that no competing interests exist.

REFERENCES

Bansal, A., Singh, S., More, K. R., Hans, D., Nangalia, K., Yogavel, M., … Chitnis, C. E. (2013). Characterization of *Plasmodium falciparum* calcium-dependent protein kinase 1 (PfCDPK1) and its role in microneme secretion during erythrocyte invasion. *The Journal of Biological Chemistry*, *288*, 1590–1602.

Berridge, M. J. (2009). Inositol tri-phosphate and calcium signalling mechanisms. *Biochimica et Biophysica Acta*, *1793*, 933–940.

Berridge, M. J., Bootman, M. D., & Roderick, H. L. (2003). Calcium: Calcium signalling: dynamics, homeostasis and remodelling. *Nature Reviews. Molecular Cell Biology*, *4*, 517–529.

Biftu, T., Feng, D., Ponpipom, M., Girotra, N., Liang, G. B., Qian, X. X., … Bugianesi, R. (2005). Synthesis and SAR of 2,3-diarylpyrrole inhibitors of parasite cGMP-dependent protein kinase as novel anticoccidial agents. *Bioorganic & Medicinal Chemistry Letters*, *15*, 3296–3301.

Billker, O., Dechamps, S., Tewari, R., Wenig, G., Franke-Fayard, B., & Brinkmann, V. (2004). Calcium and a calcium-dependent protein kinase regulate gamete formation and mosquito transmission in a malaria parasite. *Cell*, *117*, 503–514.

Billker, O., Lourido, S., & Sibley, L. D. (2009). Calcium-dependent signaling and kinases in apicomplexan parasites. *Cell Host & Microbe*, *5*, 612–622.

Black, M. W., Arrizabalaga, G., & Boothroyd, J. C. (2000). Ionophore-resistant mutants of *Toxoplasma gondii* reveal host cell permeabilization as an early event in egress. *Molecular and Cellular Biology*, *20*, 9399–9408.

Borges-Pereira, L., Budu, A., McKnight, C. A., Moore, C. A., Vella, S. A., Hortua Triana, M. A., … Moreno, S. N. J. (2015). Calcium signaling throughout the *Toxoplasma gondii* lytic cycle. A study using genetically encoded calcium indicators. *The Journal of Biological Chemistry*, *290*, 26914–26926.

Brochet, M., Collins, M. O., Smith, T. K., Thompson, E., Sebastian, S., Volkmann, K., … Billker, O. (2014). Phosphoinositide metabolism links cGMP-dependent protein kinase G to essential Ca^{2+} signals at key decision points in the life cycle of malaria parasites. *PLoS Biology*, *12*, e1001806.

Brown, K. M., Lourido, S., & Sibley, L. D. (2016). Serum albumin stimulates protein kinase G-dependent microneme secretion in *Toxoplasma gondii*. *The Journal of Biological Chemistry*, *291*, 9554–9565.

Bullen, H. E., Jia, Y., Yamaryo-Botté, Y., Bisio, H., Zhang, O., Jemelin, N. K., … Soldati-Favre, D. (2016). Phosphatidic acid-mediated signaling regulates microneme secretion in *Toxoplasma*. *Cell Host & Microbe*, *19*, 349–360.

Carey, A. F., Singer, M., Bargieri, D., Thiberge, S., Frischknecht, F., Ménard, R., & Amino, R. (2014). Calcium dynamics of *Plasmodium berghei* sporozoite motility. *Cellular Microbiology*, *16*, 768–783.

Carruthers, V. B., & Sibley, L. D. (1997). Sequential protein secretion from three distinct organelles of *Toxoplasma gondii* accompanies invasion of human fibroblasts. *European Journal of Cell Biology*, *73*, 114–123.

Carruthers, V. B., & Sibley, L. D. (1999). Mobilization of intracellular calcium stimulates microneme discharge in *Toxoplasma gondii*. *Molecular Microbiology*, *31*, 421–428.

Chen, T.-W., Wardill, T. J., Sun, Y., Pulver, S. R., Renninger, S. L., Baohan, A., … Kim, D. S. (2013). Ultrasensitive fluorescent proteins for imaging neuronal activity. *Nature*, *499*, 295–300.

Chini, E. N., Nagamune, K., Wetzel, D. M., & Sibley, L. D. (2005). Evidence that the cADPR signalling pathway controls calcium-mediated microneme secretion in *Toxoplasma gondii*. *Biochemical Journal*, *389*, 269–277.

Collins, C. R., Hackett, F., Strath, M., Penzo, M., Withers-Martinez, C., Baker, D. A., & Blackman, M. J. (2013). Malaria parasite cGMP-dependent protein kinase regulates blood stage merozoite secretory organelle discharge and egress. *PLoS Pathogens*, *9*, e1003344.

Donald, R. G. K., & Liberator, P. A. (2002). Molecular characterization of a coccidian parasite cGMP dependent protein kinase. *Molecular and Biochemical Parasitology*, *120*, 165–175.

Donald, R. G. K., Zhong, T., Wiersma, H., Nare, B., Yao, D., Lee, A., … Liberator, P. A. (2006). Anticoccidial kinase inhibitors: Identification of protein kinase targets secondary to cGMP-dependent protein kinase. *Molecular and Biochemical Parasitology*, *149*, 86–98.

Dvorin, J. D., Martyn, D. C., Patel, S. D., Grimley, J. S., Collins, C. R., Hopp, C. S., … Duraisingh, M. T. (2010). A plant-like kinase in *Plasmodium falciparum* regulates parasite egress from erythrocytes. *Science*, *328*, 910–912.

Eaton, M. S., Weiss, L. M., & Kim, K. (2006). Cyclic nucleotide kinases and tachyzoite-bradyzoite transition in *Toxoplasma gondii*. *International Journal for Parasitology*, *36*, 107–114.

Garrison, E., Treeck, M., Ehret, E., Butz, H., Garbuz, T., Oswald, B. P., … Arrizabalaga, G. (2012). A forward genetic screen reveals that calcium-dependent protein kinase 3 regulates egress in *Toxoplasma*. *PLoS Pathogens*, *8*, e1003049.

Heintzelman, M. B. (2015). Gliding motility in apicomplexan parasites. *Seminars in Cell & Developmental Biology*, *46*, 135–142.

Hortle, E., Nijagal, B., Bauer, D. C., Jensen, L. M., Ahn, S. B., Cockburn, I. A., … Burgio, G. (2016). Adenosine monophosphate deaminase 3 activation shortens erythrocyte half-life and provides malaria resistance in mice. *Blood*, *128*(9), 1290–1301.

Howard, B. L., Harvey, K. L., Stewart, R. J., Azevedo, M. F., Crabb, B. S., Jennings, I. G., … Gilson, P. R. (2015). Identification of potent phosphodiesterase inhibitors that demonstrate cyclic nucleotide-dependent functions in apicomplexan parasites. *ACS Chemical Biology*, *10*, 1145–1154.

Kafsack, B. F., Pena, J. D., Coppen, I., Ravindran, S., Boothroyd, J. C., & Carruthers, V. B. (2009). Rapid membrane disruption by a Perforin-Like Protein facilitates parasite exit from host cells. *Science*, *323*, 530–533.

Lourido, S., & Moreno, S. N. J. (2015). The calcium signaling toolkit of the apicomplexan parasites *Toxoplasma gondii* and *Plasmodium* spp. *Cell Calcium*, *57*, 186–193.

Lourido, S., Shuman, J., Zhang, C., Shokat, K. M., Hui, R., & Sibley, L. D. (2010). Calcium-dependent protein kinase 1 is an essential regulator of exocytosis in *Toxoplasma*. *Nature*, *465*, 359–362.

Lourido, S., Tang, K., & Sibley, L. D. (2012). Distinct signalling pathways control *Toxoplasma* egress and host-cell invasion. *The EMBO Journal*, *31*, 4524–4534.

Lovett, J. L., & Sibley, L. D. (2003). Intracellular calcium stores in *Toxoplasma gondii* govern invasion of host cells. *Journal of Cell Science*, *116*, 3009–3016.

Lovett, J. L., Marchesini, N., Moreno, S. N. J., & Sibley, L. D. (2002). *Toxoplasma gondii* microneme secretion involves intracellular Ca^{2+} release from inositol 1,4,5-triphosphate (IP_3)/ryanodine-sensitive stores. *The Journal of Biological Chemistry*, *277*, 25870–25876.

Luo, S., Ruiz, F. A., & Moreno, S. N. J. (2004). The acidocalcisome Ca^{2+}-ATPase (TgA1) of *Toxoplasma gondii* is required for polyphosphate storage, intracellular calcium homeostasis and virulence. *Molecular Microbiology*, *55*, 1034–1045.

McCoy, J. M., Whitehead, L., van Dooren, G. G., & Tonkin, C. J. (2012). *Tg*CDPK3 regulates calcium-dependent egress of *Toxoplasma gondii* from host cells. *PLoS Pathogens*, *8*, e1003066.

Moudy, R., Manning, T. J., & Beckers, C. J. (2001). The loss of cytoplasmic potassium upon host cell breakdown triggers egress of *Toxoplasma gondii*. *The Journal of Biological Chemistry*, *276*, 41492–41501.

Münter, S., Sabass, B., Selhuber-Unkel, C., Kudryashev, M., Hegge, S., Engel, U., … Frischknecht, F. (2009). *Plasmodium* sporozoite motility is modulated by the turnover of discrete adhesion sites. *Cell Host & Microbe*, *6*, 551–562.

Nagamune, K., Beatty, W. L., & Sibley, L. D. (2007). Artemisinin induces calcium-dependent protein secretion in the protozoan parasite *Toxoplasma gondii*. *Eukaryotic Cell*, *6*, 2147–2156.

Nagamune, K., Hicks, L. M., Fux, B., Brossier, F., Chini, E. N., & Sibley, L. D. (2008). Abscisic acid controls calcium-dependent egress and development in *Toxoplasma gondii*. *Nature*, *451*, 207–210.

Niedelman, W., Sprokholt, J. K., Clough, B., Frickel, E.-M., & Saeij, J. P. J. (2013). Cell death of gamma interferon-stimulated human fibroblasts upon *Toxoplasma gondii* infection induces early parasite egress and limits parasite replication. *Infection and Immunity*, *81*, 4341–4349.

Pappas, G., Roussos, N., & Falagas, M. E. (2009). Toxoplasmosis snapshots: Global status of *Toxoplasma gondii* seroprevalence and implications for pregnancy and congenital toxoplasmosis. *International Journal for Parasitology*, *39*, 1385–1394.

Persson, E. K., Agnarson, A. M., Lambert, H., Hitziger, N., Yagita, H., Chambers, B. J., … Grandien, A. (2007). Death receptor ligation or exposure to perforin trigger rapid egress of the intracellular parasite *Toxoplasma gondii*. *Journal of Immunology*, *179*, 8357–8365.

Roiko, M. S., Svezhova, N., & Carruthers, V. B. (2014). Acidification activates *Toxoplasma gondii* motility and egress by enhancing protein secretion and cytolytic activity. *PLoS Pathogens*, *10*, e1004488.

Sebastian, S., Brochet, M., Collins, M. O., Schwach, F., Jones, M. L., Goulding, D., … Billker, O. (2012). A *Plasmodium* calcium-dependent protein kinase controls zygote development and transmission by translationally activating repressed mRNAs. *Cell Host & Microbe*, *12*, 9–19.

Sidik, S. M., Hortua Triana, M. A., Paul, A. S., Bakkouri, El. M., Hackett, C. G., Tran, F., & Lourido, S. (2016). Using a genetically encoded sensor to identify inhibitors of *Toxoplasma gondii* Ca^{2+} signalling. *The Journal of Biological Chemistry*, *291*, 9566–9580.

Taylor, C. J., McRobert, L., & Baker, D. A. (2008). Disruption of a *Plasmodium falciparum* cyclic nucleotide phosphodiesterase gene causes aberrant gametogenesis. *Molecular Microbiology*, *69*, 110–118.

Towle, T., Chang, I., Kerns, R. J., & Bhanot, P. (2013). Chemical probes of a trisubstituted pyrrole to identify its protein target(s) in *Plasmodium* sporozoites. *Bioorganic & Medicinal Chemistry Letters*, *23*, 2812–2812.

Uhlen, P., & Fritz, N. (2010). Biochemistry of calcium oscillations. *Biochemical and Biophysical Research Communications*, *396*, 28–32.

Wernimont, A. K., Artz, J. D., Finerty, P., Lin, Y.-H., Amani, M., Allali-Hassani, A., … Hui, R. (2010). Structures of apicomplexan calcium-dependent protein kinases reveal mechanism of activation by calcium. *Nature Structural & Molecular Biology*, *17*, 596–601.

Wetzel, D. M., Chen, L. A., Ruiz, F. A., Moreno, S. N. J., & Sibley, L. D. (2004). Calcium-mediated protein secretion potentiates motility in *Toxoplasma gondii*. *Journal of Cell Science*, *117*, 5739–5748.

Wiersma, H. I., Galuska, S. E., Tomley, F. M., Sibley, L. D., Liberator, P. A., & Donald, R. G. K. (2004). A role for coccidian cGMP-dependent protein kinase in motility and invasion. *International Journal for Parasitology*, *34*, 369–380.

Williams, M. J., Alonso, H., Enciso, M., Egarter, S., Sheiner, L., Meissner, M., … Tonkin, C. J. (2015). Two essential light chains regulate the MyoA lever arm to promote T*oxopalsma* gliding motility. *mBio*, *6*, e00845–e00815.

World Health Organization (2014) report 2014. 1–242.

SUPPORTING INFORMATION

Additional Supporting Information may be found online in the supporting information tab for this article.

How to cite this article: Stewart RJ, Whitehead L, Nijagal B, et al. Analysis of Ca^{2+} mediated signaling regulating *Toxoplasma* infectivity reveals complex relationships between key molecules. *Cellular Microbiology*. 2017;**19**:e12685. https://doi.org/10.1111/cmi.12685